Frequency Selection and Calibration of a Water Vapor Radiometer

S. C. Wu
Tracking Systems and Applications Section

The calibration coefficients of existing water vapor radiometers are dependent upon meteorology profiles. This is shown to be due mainly to incorrect frequency pairs. By properly selecting an optimum frequency pair, the dependency can be reduced to a relatively small amount which can be handily adjusted by surface measurement alone. Hence, a universal calibration equation is applicable to all environmental conditions – site, seasonal and diurnal variations. Optimum frequency pairs are systematically searched. Error analysis indicates that calibration for the water vapor phase delay accurate to <2 cm is possible at all elevation angles >15 degrees.

I. Introduction

Tropospheric water-vapor phase delay calibration by means of a ground based water-vapor radiometer (WVR) has long been desired. During the last several years, investigations of dual-frequency WVRs (Refs. 1,2) have been carried out. It has been demonstrated that under "ideal" weather conditions SMILE[1] (Ref. 1) provides a calibration to better than 2 cm for elevation angles down to 10 deg; under "adverse" weather conditions the error is 3 to 5 times worse. It was felt that probably no single set of calibration coefficients can be applied to all weather types.

The frequency pairs for the two radiometers are such that one channel is centered right at the water-vapor resonance frequency of 22.235 GHz, with the other channel centered at a frequency outside of the resonance band. For SMILE in Reference 1, the second frequency is 31.4 GHz, while for the Deep Space Network (DSN) prototype in Reference 2 it is 18.5 GHz. The frequency pairs so selected have the advantage of high sensitivity to the variation of water-vapor content. However, it will be seen in the following analysis that such frequency pairs have an undesirable high degree of dependence on meteorology profiles. This is due to the unequal contribution of the differential water-vapor phase delay along the ray path and to the lack of means to correct for different weather types.

Menius et al. (Ref. 4) found that there exists a frequency on each side of the water-vapor resonance line at which the profile dependence is minimal. Gaut (Ref. 5) improved the dependence by linear combination of two or three frequencies. This approach is ideal when there is no cloud (liquid water droplets). The existence of cloud in the atmosphere may result in significant error in the inferred phase delay. In this paper, a *constrained* dual-frequency approach is adopted. The constraint is such that the radiations due to liquid water at the two frequencies cancel one another when linearly combined.

Minimizing the profile dependence is no more than equalizing the weight on each differential water vapor phase delay

[1] Scanning Microwave Inversion Layer Experiment Radiometer, a unit similar to SCAMS (Ref. 3) but only two of the five channels are used.

along the ray path. With such constant weight, the residual dependence of the calibration coefficients on the environmental conditions can be handily corrected for by surface measurement alone: the weight at the surface is factored out as an additional observable so that a set of universal calibration coefficients is applicable under all circumstances – independent of site, season, profiles, and diurnal variation.

II. Weighting Function

The phase delay due to water vapor is

$$\Delta\rho = k \int_0^\infty \frac{\sigma}{T} dS, \qquad k = 1.723 \times 10^{-3}\ \mathrm{K/(g/m^3)} \quad (1)$$

where σ and T are the density and temperature of water vapor along the ray path S. On the other hand, the brightness temperature of a ground-based radiometer at a frequency f due to the same water vapor, to oxygen and to cloud is

$$T_B = T_c\, e^{-\tau_\infty} + \int_0^\infty T \alpha\, e^{-\tau}\, dS \quad (2)$$

where

$$\tau_\infty = \int_0^\infty \alpha\, dS$$

is the opacity of the atmosphere,

$$\tau = \int_0^S \alpha\, dS$$

T_c is the cosmic noise of ~ 2.9K and α is the total absorption coefficient of the constituents along the ray path, $\alpha = \alpha_v + \alpha_0 + \alpha_l$, with v, o and l denoting the water vapor, the oxygen and the liquid water respectively.

For a dual-frequency radiometer, the two brightness temperatures are

$$T_{B,1} = T_{c,1} + \int_0^\infty T\alpha_1\, e^{-\tau_1}\, dS$$
$$T_{B,2} = T_{c,2} + \int_0^\infty T\alpha_2\, e^{-\tau_2}\, dS \quad (3)$$

where the attenuated cosmic-noise terms have been replaced by two constants $T_{c,1}$ and $T_{c,2}$. This is valid since $T_c \ll T_B$ and the opacity $\tau_\infty \ll 1$ for frequencies $f < 40$ GHz. In this frequency range, the absorption coefficient of cloud α_c is proportional to f^2 (Ref. 6). Hence, from Eq. (3), we have

$$\frac{T_{B,1} - T_{C,1}}{f_1^2} - \frac{T_{B,2} - T_{C,2}}{f_2^2} = \int_0^\infty W(S) \frac{\sigma}{T} dS + T_0 \quad (4)$$

where

$$W(S) = \frac{T^2}{\sigma}\left[\frac{\alpha_{v,1}}{f_1^2} e^{-\tau_1} - \frac{\alpha_{v,2}}{f_2^2} e^{-\tau_2}\right] \quad (5)$$

and

$$T_0 = \int_0^\infty T\left[\frac{\alpha_{0,1}}{f_1^2} e^{-\tau_1} - \frac{\alpha_{0,2}}{f_2^2} e^{-\tau_2}\right] dS \quad (6)$$

By comparing Eqs. (1) and (4) it is obvious that $W(S)$ is a weighting function with which the incremental water-vapor phase delays are summed to a quantity proportional to the linear combination of the two brightness temperatures $T_{B,1}$ and $T_{B,2}$. A nonconstant $W(S)$ implies nonuniqueness of phase delay inferred by the linear combination of $T_{B,1}$ and $T_{B,2}$:

$$\Delta\rho = a_0 + a_1 T_{B,1} + a_2 T_{B,2} \quad (7)$$

In other words, the coefficients a_0, a_1 and a_2 are functions of the profile of σ/T. If $W(S) = W_m$, a constant, then Eq. (4) reduces to Eq. (7) with constant coefficients:

$$a_0 = [T_{c,2}/f_2^2 - T_{c,1}/f_1^2 - T_0]\ k/W_m$$
$$a_1 = k/f_1^2\, W_m \quad (8)$$
$$a_2 = -k/f_2^2\, W_m$$

III. Modified Weighting Function and Linearized Brightness Temperature

The weighting function defined in Eq. (5) may be constant at low air masses for which τ_1 and τ_2 are small. For high air masses, these quantities increase rapidly and the two terms in the bracket of Eq. (5) will decrease with S and hence $W(S)$ will

be lower at larger S. To maintain constant $W(S)$ it is desirable not to have such exponential terms in Eq. (5). This is possible if the brightness temperatures are "linearized"

The "linearized" brightness temperature is *defined* as

$$T_B' \equiv T_c \left(1 - \int_0^\infty \alpha\, dS\right) + \int_0^\infty T\alpha\, dS \qquad (9)$$

$$= T_c + \int_0^\infty (T - T_c)\,\alpha\, dS \qquad (10)$$

Following the procedures of the previous section, we arrive at the difference of the brightness temperatures in Eq. (10) for frequencies f_1 and f_2 respectively:

$$\frac{T_{B,1}' - T_c}{f_1^2} - \frac{T_{B,2}' - T_c}{f_2^2} = \int_0^\infty W'(S)\,\frac{\sigma}{T}\,dS + T_0' \qquad (11)$$

where the weighting function is now modified to be

$$W'(S) = \frac{T(T - T_c)}{\sigma}\left[\frac{\alpha_{v,1}}{f_1^2} - \frac{\alpha_{v,2}}{f_2^2}\right] \qquad (12)$$

and where

$$T_0' = \int_0^\infty (T - T_c)\left[\frac{\alpha_{0,1}}{f_1^2} - \frac{\alpha_{0,2}}{f_2^2}\right] dS \qquad (13)$$

This weighting function does not have the exponential terms as in Eq. (5). This implies that $W'(S)$ as defined in Eq. (12) is identical for all air masses; a constant $W'(S)$ for a zenith ray path will also be constant for lower elevation angles as long as homogeneity exists.

For a constant $W'(S) = W_m'$, Eq. (11) reduces to

$$\Delta\rho = a_0 + a_1 T_{B,1}' + a_2 T_{B,2}' \qquad (14)$$

with

$$a_0 = [T_c (f_2^{-2} - f_1^{-2}) - T_0']\; k/W_m'$$

$$a_1 = k/W_m' f_1^2, \qquad (15)$$

$$a_2 = -k/W_m' f_2^2.$$

The T_0' included in a_0 is a quantity proportional to the number of air masses. It is practically constant for small air masses: the absorption coefficient of oxygen is proportional to $P^2 T^{-2.85}$ (Ref. 6); tropospheric P and T profiles can be represented by standard models with ±3% variation in P and ±10% variation in T. Hence the error in $T\alpha_0$ is within 27%. The proportionality of α_0 with frequency squared is better than 60%. Therefore, the quantity $T(\alpha_{0,1}/f_1^2 - \alpha_{0,2}/f_2^2)$, and hence T_0', is constant to within 11%. This corresponds to <1 mm error in $\Delta\rho$ for a zenith ray path. For ray paths at low elevation angles adjustment is needed as will be described later.

In Eq. (14) it is the "linearized" brightness temperatures $T_{B,1}'$ and $T_{B,2}'$ that are used to infer the phase delay $\Delta\rho$ due to atmospheric water vapor. On the other hand, the quantities that are measured are the "saturated" brightness temperatures $T_{B,1}$ and $T_{B,2}$. Fortunately, T_B' can be calculated from T_B to high accuracy. Equations (2) and (9) can be rewritten as

$$T_B = T_c\, e^{-\tau_\infty} + T_{eff}(1 - e^{-\tau_\infty}) \qquad (16)$$

and

$$T_B' = T_c (1 - \tau_\infty) + T_{eff}'\, \tau_\infty \qquad (17)$$

where T_{eff} and T_{eff}' are effective temperatures in Eqs. (2) and (9) respectively, defined as

$$T_{eff} = \frac{\int_0^\infty T\alpha e^{-\tau}\, dS}{\int_0^\infty \alpha e^{-\tau}\, dS} \qquad (18)$$

and

$$T_{eff}' = \frac{\int_0^\infty T\alpha\, dS}{\int_0^\infty \alpha\, dS} \qquad (19)$$

T_{eff} and T_{eff}' are highly correlated and can be connected by $T_{eff} \doteq (1 + Q)\, T_{eff}'$, as will be seen later.

Eliminating τ_∞ between (16) and (17) yields

$$T_B' = T_c - (T_{eff}' - T_c) \ln\left(1 - \frac{T_B - T_c}{T_{eff} - T_c}\right) \qquad (20)$$

It is easy to show, for the case $Q = 0$ (i.e., $T'_{eff} = T_{eff}$), that a 10 K error in T_{eff} will result in only < 1 K error in T'_B. This is also true for $Q \ll 1$. Hence T'_B can be calculated from T_B even with a T_{eff} not well estimated. Study indicates that T_{eff} can be estimated to better than 5 K from the surface temperature alone, as will be seen later.

IV. Optimum Frequency Search

In this section, frequency pairs for which $W'(S)$ remains nearly constant along the ray path are to be sought. Since water vapor concentrates almost exclusively at altitudes below 6 km, a nearly constant $W'(S)$ over only this altitude range is of concern. The searching labor can be reduced by first examining the two components of the weighting function in Eq. (12) separately. The pairs having similar variations with ray path can be picked out as possible candidates. The weighting functions $W'(S)$ for these candidates are then calculated for further comparison.

Another factor to be considered is the sensitivity of the inferred phase delay to the error in measured brightness temperatures. This can be shown to be inversely proportional to the magnitude W'_m: Let $\delta_{T'_B}$ be the error in $T'_{B,1}$ and $T'_{B,2}$. Then the error in $\Delta\rho$ from Eq. (14), assuming uncorrelated errors in $T'_{B,1}$ and $T'_{B,2}$, is

$$\epsilon_{T'_B} = (a_1^2 + a_2^2)^{1/2} \delta_{T'_B}$$

$$= \frac{k}{W'_m} \left(\frac{1}{f_1^4} + \frac{1}{f_2^4} \right)^{1/2} \delta_{T'_B} \equiv \beta \delta_{T'_B} \qquad (21)$$

Therefore, in selecting the optimum frequency pair, a compromise between constant $W'(S)$ and a minimum error factor $\beta \equiv k W'^{-1}_m (f_1^{-4} + f_2^{-4})^{1/2}$ has to be made. In other words, an optimum frequency pair will have constant as well as large $W'(S)$.

For the calculation, radiosonde measurement of the meteorology profiles at Point Mugu, California, on February 24, 1976, is selected arbitrarily. These profiles are shown in Fig. 1. It will be demonstrated later that for a specific frequency pair, the shape of weighting function is similar for different profile shapes. Hence it is sufficient to examine the profiles of only one radiosonde launch. The weighting function components $T(T - T_c)\alpha_v/\sigma f^2$ are calculated and plotted in Fig. 2 for frequencies within the range of 18.5 to 31.4 GHz. Any pair having equal vertical distance in Fig. 2 will have a constant $W'(S)$. It is obvious that the resonance frequency 22.235 GHz can only be paired with frequencies very close to itself, which would result in singularity (large $\epsilon_{T'_B}$ as indicated by Eq. 21). The pair having the largest and most constant vertical separation turns out to be 20.3 and 31.4 GHz. The higher frequency can be varied by ±2 GHz without appreciably affecting the results. Other possible pairs are 20.0/26.5 GHz, 24.5/31.4 GHz, etc.

The variations of the normalized weighting functions $[W'(S) - W'(0)]/W'(0)$ are plotted in Fig. 3 for these three candidates. The DSN prototype (22.235/18.5 GHz) and the SMILE (22.235/31.4 GHz) are also included for comparison. It is seen that the existing radiometers have large variation in $W'(S)$ and hence their calibration coefficients are profile-dependent.

The three frequency pairs selected have very similar shapes in $W'(S)$ which are constant to within 5% for all altitudes <5 km where most water vapor resides. The pair 20.3/31.4 GHz has a slightly better error factor β (as defined in Eq. 21) than the other two pairs, and the choices are heavily dependent upon hardware availability and simplicity. For instance, the pair 20.0/26.5 GHz is convenient since a common waveguide may be shared by the two channels.

To further demonstrate the above features, data from two more radiosonde launches are selected. These launches are carefully selected to represent two completely different weather conditions from the preceding analysis, a dry day (3/12/76) and a day with high-altitude water vapor concentration (3/16/76), again at Point Mugu. The profiles are shown in Figs. 4 and 5. The resulting weighting functions are plotted in Fig. 6. It is seen that the constancy of these weighting functions does not show any degradation under such extreme weather conditions. It is believed that with these frequency pairs the weighting functions will remain within a range ±10% of their surface values for all weather conditions.

V. Adjustments of Calibration Coefficients

It has been desired to have a simple means to adjust the calibration coefficients a_0, a_1 and a_2 in Eq. (15) to cover different ground altitudes as well as diurnal and seasonal variations of temperature. Having a constant $W'(S)$ along a ray path S implies that the adjustment factor, in this case the mean weighting function W'_m, is simply $W'(0)$, a quantity which can be calculated by surface measurement alone (cf Eq. 12). In practice, the adjustment can be avoided by factoring out the weighting function W'_m in Eqs. (14):

$$\Delta\rho = (b_0 + b_1 T'_{B,1} + b_2 T'_{B,2})/W'_m \qquad (22)$$

A set of nominal calibration coefficients b_0, b_1 and b_2 is determined by a constrained linear least-squares fit[2] of Eq. (22) with actual measurement of $\Delta\rho, T'_{B,1}, T'_{B,2}$ and $W'_m = W'(0)$, the surface value of the weighting function. These coefficients are independent of W'_m and hence will remain constant under all conditions. When inferring $\Delta\rho$ from $T'_{B,1}$ and $T'_{B,2}$ of a dual-frequency radiometer, Eq. (22) is used with W'_m being the weighting function calculated from surface measurement only.

When the radiometer is making brightness temperatures measurement at more than one air mass, at extreme temperature and/or at an altitude different appreciably from where it was calibrated, the oxygen radiation term T'_0 included in b_0 (cf Eqs. 14, 15 and 22), will have to be corrected. A simple means to do this is to separate T'_0 from the cosmic-noise term $T_c(f_2^{-2} - f_1^{-2})$ and adjust T'_0 by the number of air masses m, the surface pressure P_S and the surface temperature T_S. The absorption coefficient of oxygen is proportional to $P^2T^{-2.85}$ (Ref. 6) and T'_0 in Eq. (13) is nearly proportional to $P^2T^{-1.85}$. Hence

$$\begin{aligned} b_{0,\,\text{corrected}} &= [b_0 - kT_c\,(f_2^{-2} - f_1^{-2})]\; m\,(P_s/\bar{P})^2\,(\bar{T}/T_s)^{1.85} \\ &\quad + kT_c(f_2^{-2} - f_1^{-2}) \\ &= G\,b_0 + T_c\,(G-1)\,(b_1 + b_2) \end{aligned} \tag{23}$$

where

$$G = m(P_s/\bar{P})^2\,(\bar{T}/T_s)^{1.85} \tag{24}$$

with m being the air masses and $\bar{P}$ and $\bar{T}$ being the mean surface pressure and temperature of the radiosonde launches, which are used in the determination of b_0, b_1 and b_2 by the least-squares fit. b_1 and b_2 will remain fixed under all circumstances.

VI. Estimation of Effective Temperatures

An accurate calculation of "linearized" brightness temperature requires a sufficiently accurate (< 5 K) estimate of the effective temperatures defined in Eqs. (18) and (19). T'_{eff} in Eq. (19) is independent of the number of air masses while T_{eff} in Eq. (18) is larger for large m, due to lower weight (as compared to that for T'_{eff}) at higher altitudes where T is smaller. Study of 25 soundings from Point Mugu indicates that $T_{eff} \doteq (1 + 0.0009\text{m})\,T'_{eff}$ with a standard deviation of ~0.06 K. Also found in analyzing these 25 soundings is the correlation between T'_{eff} and the surface temperature T_S: $T'_{eff} \doteq 0.950T_S$ for 20.0, 20.3 and 24.5 GHz, $T'_{eff} = 0.946T_S$ for 26.5 GHz and $T'_{eff} \doteq 0.940T_S$ for 31.4 GHz with standard deviations of < 3.5K. Another correlation found is that the errors in calculated T'_{eff} and T_{eff} are always in the same direction and nearly equal for the two frequencies used in a radiometer. This reduces the impact on the accuracy of the calculated range change through Eq. (22) since b_1 and b_2 have opposite signs. With the error in T'_{eff} and T_{eff} specified above, the error in $\Delta\rho$ will be ~ 0.2 cm for both frequency pairs at elevation angles down to $\gamma = 10°$. At higher elevation angles the error will reduce according to $1/\sin\gamma$.

VII. Demonstration of Phase Delay Determination

The same 25 soundings are used to determine the calibration coefficients b_0, b_1 and b_2 by least squares fitting Eq. (22) at $\gamma = 90°$. These are listed in Table 1 for the three optimum frequency pairs and for the pair 22.235/18.5 GHz of one of the existing WVR. In the least-squares fits the constraint $b_1/b_2 = -(f_2/f_1)^2$ has been enforced to explicitly remove the effect of cloud. This will not be needed if actual brightness temperatures (containing cloud effect) measured by a radiometer are used in place of calculated brightness temperatures (not containing cloud effect) from radiosonde profiles.

The calibration coefficients are used to calculate $\Delta\rho$ at zenith as well as at 10 deg elevation angle and then subtracted by the measured $\Delta\rho$ to indicate the error in the calculated $\Delta\rho$. These are summarized in Table 2. The same sets of calibration coefficients, which have been determined from Point Mugu data, are applied to 21 radiosonde launches at Edwards AFB, taken randomly over the whole year. The results are also shown in Table 2. The three optimum frequency pairs result in very similar solutions, which are all better than the 22.235/18.5 GHz pair by a factor of 4 to 6. The results at Point Mugu are somewhat overoptimistic since they are the result of forced fitting between the two sets of "measurements." On the other hand, the results at Edwards AFB are free from forced-fitting effect and are more objective. Hence, in the following error analysis, results at Edwards AFB only will be used.

The above errors are mostly due to nonconstant weighting functions, with a slight contribution from the imperfect effective temperature estimation. Other error sources which have to be considered in the WVR design include brightness temperature measurement error, elevation angle (antenna

[2] With the constraint $b_1/b_2 = -(f_2/f_1)^2$ to remove the effect of cloud.

pointing) error, and radiosonde measurement[3] error. The calculations of these error components are outlined in the Appendix. Figure 7 shows the $\Delta\rho$ error components for the four frequency pairs. The dominant error source for the existing WVR (22.235/18.5 GHz) is that due to nonconstant weighting function. With optimum frequency pairs this error source is reduced to an amount smaller than that due to radiosonde measurement. The total RSS errors in $\Delta\rho$ are compared in Fig. 8. The optimum systems have an RSS error of <2 cm for all elevation angles >15 deg. The existing system has an error >2 cm for elevation angles <42 deg.

The error source from radiosonde measurement can be reduced by using more launches in the determination of calibration coefficients. Currently the use of "two-color" (optical-radio) ranging system is under consideration as a perfect calibration standard in place of radiosonde. With such calibration standard, the error source marked RADIOSONDE in Fig. 7 is essentially zero. This improves the current system only slightly (being not a major error source), while it improves the optimum systems considerably (being a major error source).

[3]Radiosonde measurement is needed in the determination of calibration coefficients through least-squares fit, since accurate measurement of atmospheric absorption coefficients is not available.

VIII. Conclusion

Three frequency pairs have been found to have nearly constant weighting functions along a ray path. These are: 20.3/31.4 GHz, 20.0/26.5 GHz and 24.5/31.4 GHz. The 31.4 GHz can be varied by ±2 GHz and the 26.5 GHz by ±1 GHz without appreciably affecting the results. The constancy of the weighting functions reduces WVR error in two respects: (1) it reduces the profile dependence of the calibration coefficients and (2) it makes possible accurate adjustment of coefficients by surface measurement alone to account for different environmental conditions (site, season, diurnal variation, etc.). With such weighting function constancy, a single set of universal calibration coefficients is applicable throughout.

With any of these optimum frequency pairs, a WVR is capable of inferring the tropospheric water-vapor phase delay to <2 cm accuracy for all elevation angles >15 deg. The accuracy can be further improved by using better calibration standard in place of radiosonde launches, e.g., an optical–radio ranging system.

References

1. Winn, F. B., et al., "Atmospheric Water Vapor Calibrations: Radiometer Techniques," *DSN Progress Report 42-32*, Jet Propulsion Laboratory, Pasadena, Calif., Apr. 15, 1976, pp. 38-49.
2. Slobin, S. D., and Batelaan, P. D., "DSN Water Vapor Radiometer Development – A Summary of Recent Work, 1976-1977," *DSN Progress Report 42-40*, Jet Propulsion Laboratory, Pasadena, Calif., Aug. 14, 1977, pp. 71-75.
3. Staelin, D. H., et al., "The Scanning Microwave Spectrometer (SCAMS) Experiment," *Nimbus 6 User's Guide*, Goddard Space Flight Center, 1975.
4. Menius, A. C., et al., "Tropospheric Refraction Corrections Using a Microwave Radiometer," Technical Staff Technical Memo, No. 19, ETV-TM-64-12, Pan American Airways. Nov. 16, 1964.
5. Gaut, N. E., "Study of Atmospheric Water Vapor by Means of Passive Microwave Techniques". Technical Report 467, MIT Research Laboratory of Electronics, Dec. 20, 1968.
6. Van Vleck, J. H., et al., "Atmospheric Attenuation," *Propagation of Short Radio Waves*, D. E. Kerr, ed., McGraw-Hill, 1951, Chapter 8.

Table 1. Calibration coefficients determined from 25 radiosonde launches at Point Magu, California

Frequency pair	b_0	b_1	b_2	β
22.235/18.5 GHz	0.814	0.184	−0.265	0.98
20.3/31.4 GHz	−1.13	0.419	−0.175	0.82
20.0/26.5 GHz	−0.945	0.432	−0.246	1.35
24.5/31.4 GHz	−0.455	0.289	−0.176	0.97

b_0 is in $(10^{-5})K^2/(g/m^3)/(GHz)^2$

b_1 and b_2 are in $(10^{-5})K/(g/m^3)/(GHz)^2$

$\beta = (b_1^2 + b_2^2)^{1/2}/\overline{W}'_m$ is in cm/K

Table 2. Error in calculated $\Delta\rho$, assuming perfect radiosonde and T_B Measurement; calibration coefficients determined from Point Mugu Data

Frequency pair	Point Mugu (25 launches)		Edwards AFB (21 launches)	
	γ=90°	γ=10°	γ=90°	γ=10°
22.235/18.5 GHz	0.79 cm	4.39 cm	1.27 cm	6.90 cm
20.3/31.4 GHz	0.13	0.84	0.28	1.65
20.0/26.5 GHz	0.14	0.83	0.28	1.38
24.5/31.4 GHz	0.14	0.88	0.30	1.76

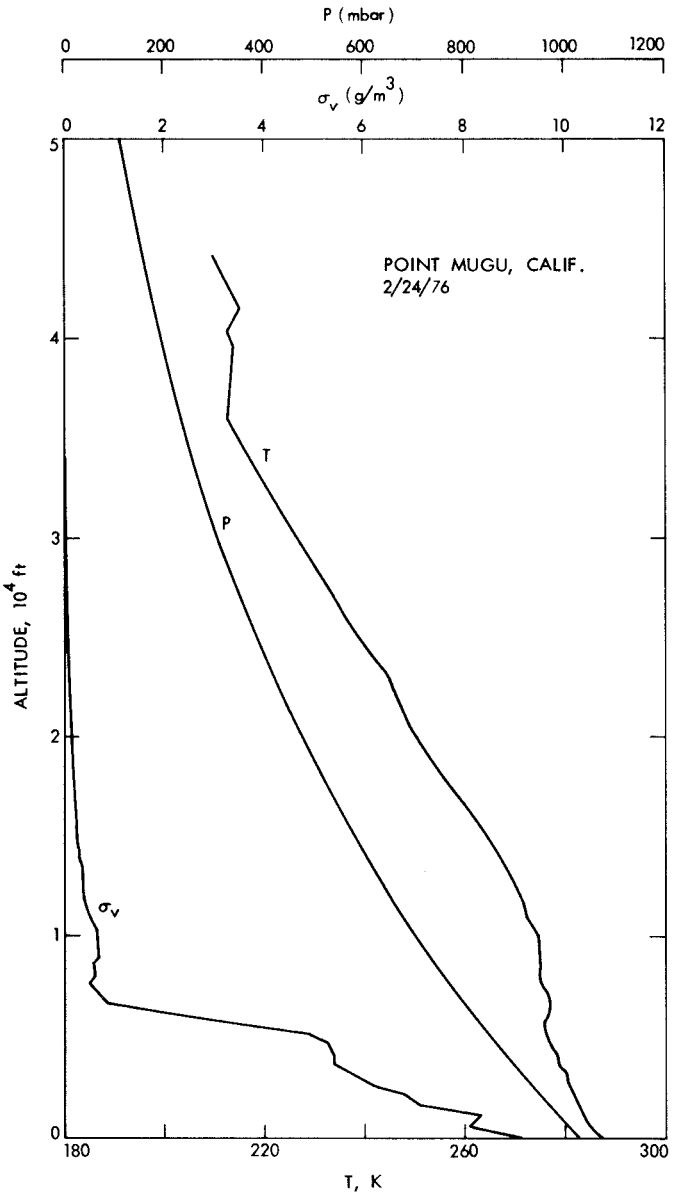

Fig. 1. Typical profiles of atmospheric temperature, pressure and water-vapor density

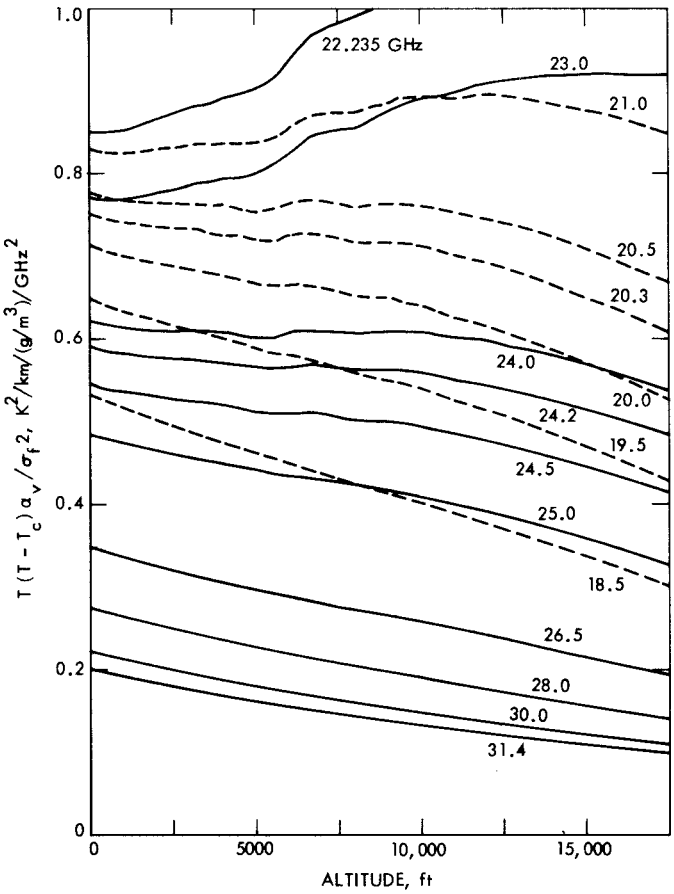

Fig. 2. Components of weighting functions for various frequencies

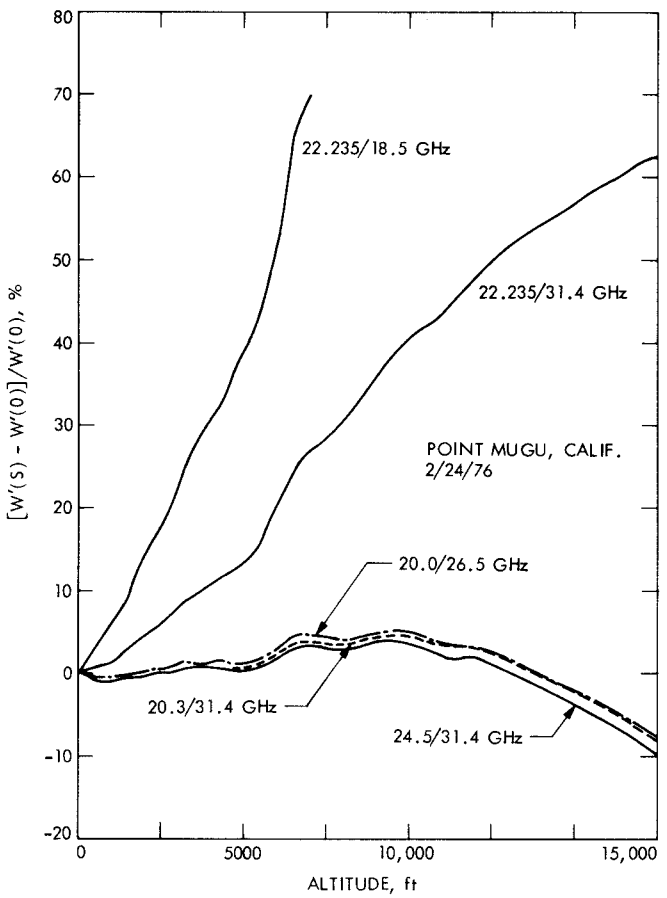

Fig. 3. Normalized weighting functions for various frequency pairs

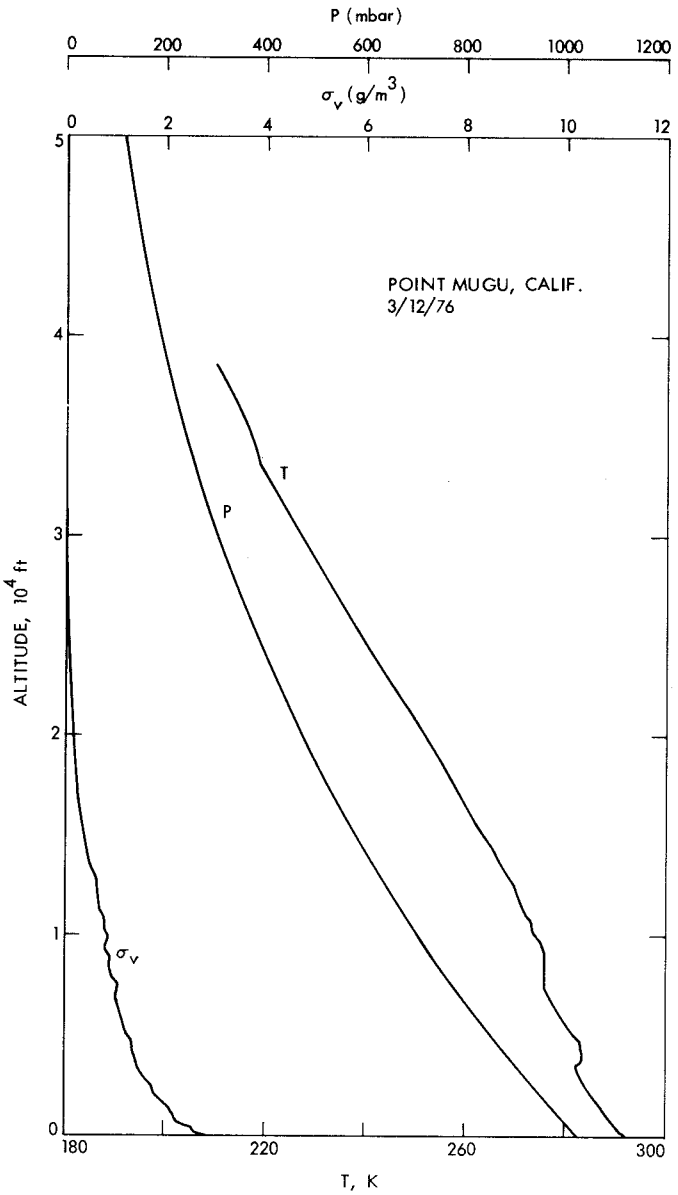

Fig. 4. Profiles of atmospheric temperature, pressure and water-vapor density for a dry day

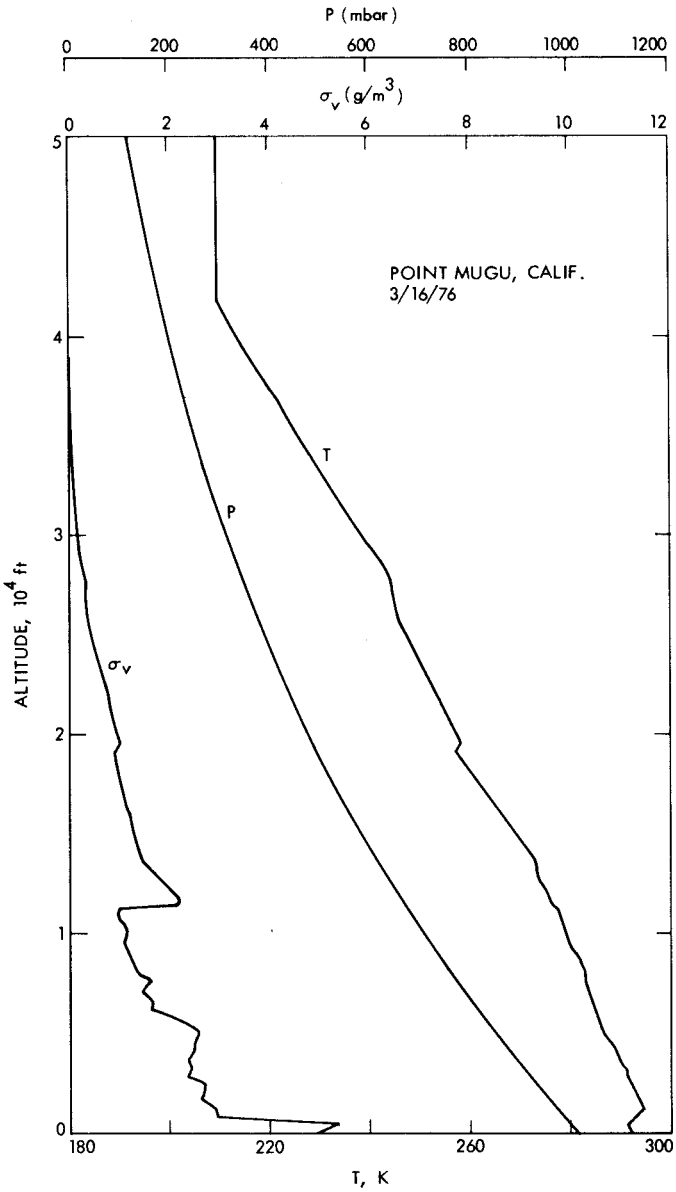

Fig. 5. Profiles of atmospheric temperature, pressure and water-vapor density for a day having high-altitude concentration of water vapor

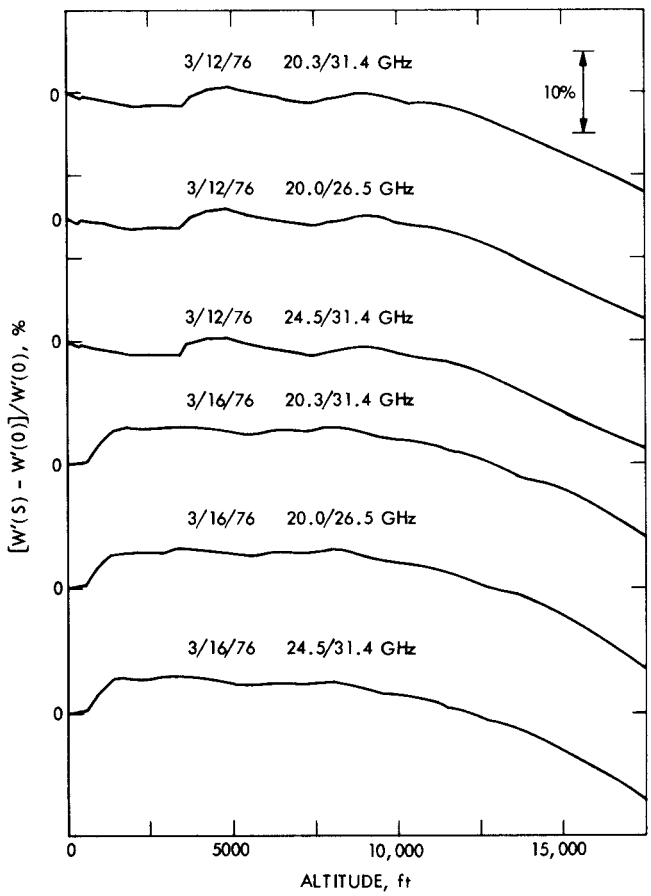

Fig. 6. Normalized weighting functions under extreme weather conditions

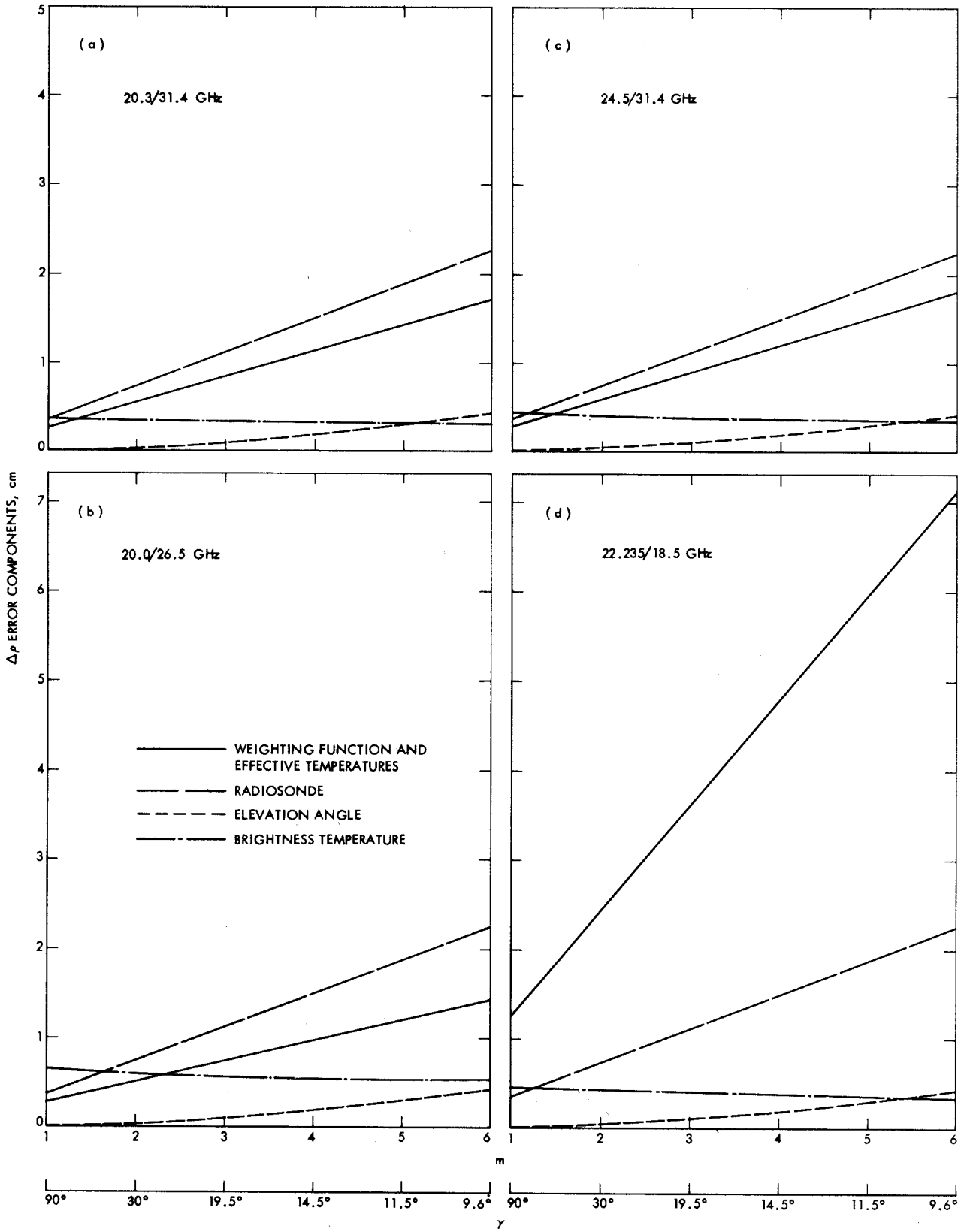

Fig. 7. Components of error in water-vapor phase delay inferred by a dual-frequency WVR

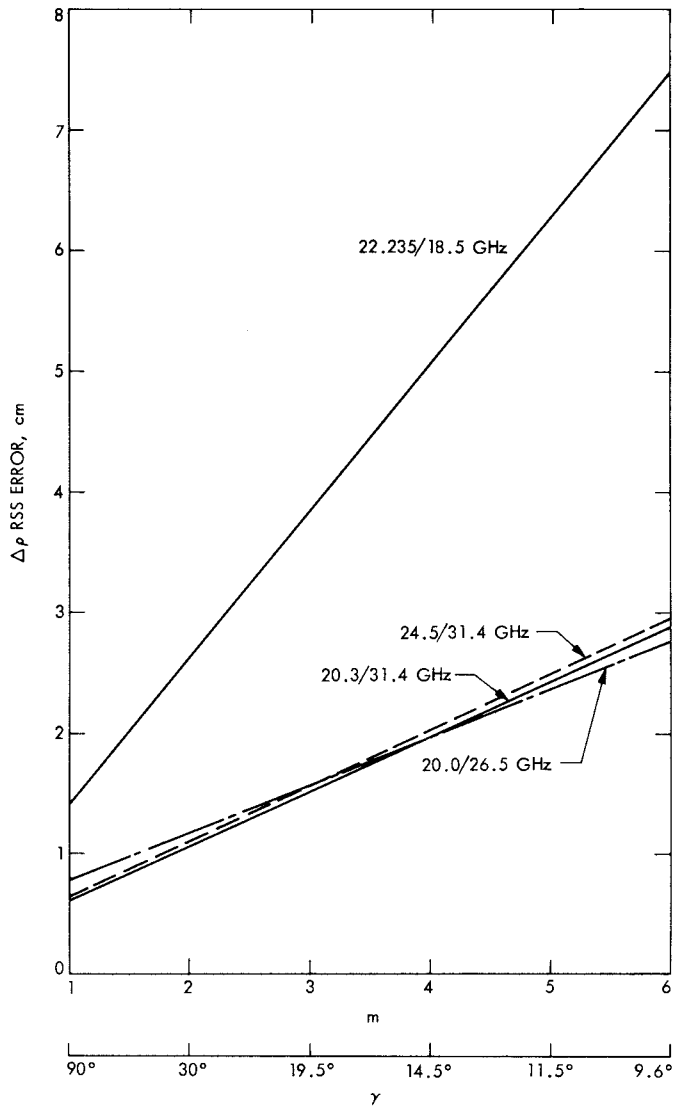

Fig. 8. Total RSS error in water-vapor phase delay inferred by a dual-frequency WVR

Appendix

Error Component Calculations

A. Nonconstant Weighting Functions and Imperfect Effective Temperatures:

The errors calculated in the last two columns of Table 2 (at Edwards AFB) using coefficients derived at Pt. Mugu are adopted with the assumption that they increase linearly with air masses between 1 and 6.

B. Radiosonde:

Assume: 1 cm random error in each launch (along zenith), increases with air masses (m).

$$\text{Number of launches} = n_l = 21$$

$$\text{Number of coefficients} = n_c = 3$$

$$\epsilon_{\text{radiosonde}} = 1.0\, m/(n_l/n_c)^{1/2}$$

$$= 0.378\, m \quad \text{(cm)}$$

C. Elevation Angle (Antenna Pointing):

Assume: Error in elevation angle $\epsilon_\gamma = 0.1°$. Zenith phase delay $\Delta\rho_z = 7$ cm (mean value of 46 soundings in Table 2).

$$\epsilon_{\text{elevation}} = \left| \frac{\partial}{\partial\gamma}\left(\frac{\Delta\rho_z}{\sin\gamma}\right) \right| \epsilon_\gamma$$

$$= (7\cos\gamma/\sin^2\gamma)\,(0.1\,\pi/180)$$

$$= 0.0122\, m(m^2 - 1)^{1/2}\,, m = 1/\sin\gamma$$

D. Brightness Temperature Measurement (T_B'):

Assume: Hot load has a nominal temperature $T_H = 450$ K with a long-term absolute uncertainty of ±1 K and a short term jitter of ±0.2 K. Ambient load has a nominal temperature $T_M = 300$ K with a long-term absolute uncertainty of ±0.5 K and a short-term jitter of ±0.1 K.

Calibration line equation:

$$T_B' = T_M + \frac{T_H - T_M}{N_H - N_M}(N_M - N_B)$$

where N's are the radiometer digital "counts."

$$\frac{\partial T_B'}{\partial T_H} = -\left(\frac{T_M - T_B'}{T_H - T_M}\right) = -\left(\frac{300 - T_B'}{150}\right)$$

$$\frac{\partial T_B'}{\partial T_M} = 1 + \left(\frac{T_M - T_B'}{T_H - T_M}\right) = \frac{450 - T_B'}{150}$$

The hot load long-term uncertainty is correlated to ambient load long-term uncertainty by using tipping curve so that (cf. Fig. A-1).

$$\sigma_H/\sigma_M = \frac{T_H - 2.9}{T_B - 2.9} = 1.5$$

$$\sigma_H = 1.5\,\sigma_M = 0.75 \text{ K}$$

The error in T_B' due to these correlated uncertainties is

$$\epsilon_c = \left| \frac{\partial T_B'}{\partial T_H}\sigma_H + \frac{\partial T_B'}{\partial T_M}\sigma_M \right|$$

$$= \left| \frac{-(300 - T_B')}{150}(0.75) + \frac{450 - T_B'}{150}(0.5) \right|$$

$$= 0.25\, T_B'/150$$

The error in T_B' due to the uncorrelated jitter[4] in T_H and in T_M is

$$\epsilon_u = \left[\left(\frac{\partial T_B'}{\partial T_H}0.2\right)^2 + \left(\frac{\partial T_B'}{\partial T_M}0.1\right)^2\right]^{1/2}$$

[4] To reduce the effect of receiver gain drift it is necessary to repeat the "internal calibration" by looking at T_H and T_M once in a while.

$$= \left[\frac{(300 - T_B')^2}{150^2}(0.2)^2 + \frac{(450 - T_B')^2}{150^2}(0.1)^2\right]^{1/2}$$

$$= (0.05\,T_B'^2 - 33\,T_B' + 5625)^{1/2}/150$$

The total error in T_B' is the RSS of ϵ_c and ϵ_u:

$$\epsilon_{c+u} = (\epsilon_c^2 + \epsilon_u^2)^{1/2}$$

$$= (0.1125\,T_B'^2 - 33T_B' + 5625)^{1/2}/150$$

The calibration equation is (Eq. 22).

$$\Delta\rho = (b_0 + b_1\,T_{B,1}' + T_{B,2}')/W_m'$$

The typical values for b_1/W_m', b_2/W_m', and $T_{B,1}'$, $T_{B,2}'$ for the four systems are:

f_1/f_2	b_1/W_m'	b_2/W_m'	$T_{B,1}'$	$T_{B,2}'$
22.235/18.5	0.559	-0.805	30 m	15 m
20.3/31.4	0.754	-0.315	20	19
20.0/26.5	1.174	-0.668	20	19
24.5/31.4	0.826	-0.503	23	19

where m is the number of air masses.

The error in $\Delta\rho$ due to error in T_B' is:

$$\epsilon_{T_B'} = \left[\left(\frac{b_1}{W_m'}\epsilon_{c+u|T_{B,1}'}\right)^2 + \left(\frac{b_2}{W_m'}\epsilon_{c+u|T_{B,2}'}\right)^2\right]^{1/2}$$

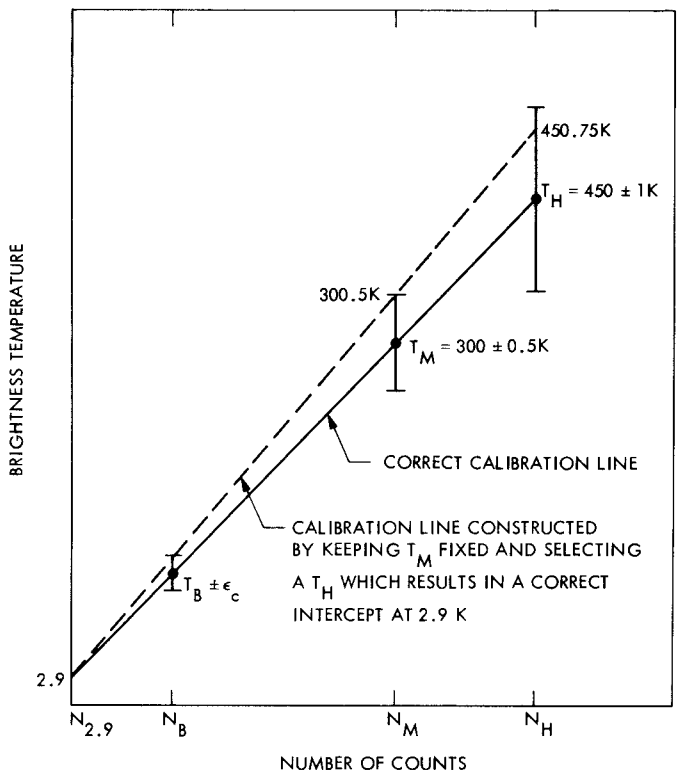

Fig. A-1. Error in linearized brightness temperature due to correlated long-term absolute uncertainties in hot-load and ambient-load temperatures